

Improving pile-up handling in the Mu2e calorimeter MC

P. Murat (Fermilab), S. R. Soleti (Sapienza - Università di Roma)

Abstract

In a pileup-dominated Mu2e environment, reconstruction of the conversion electron clusters in the calorimeter is affected by the presence of the background hits overlapping in space and time with hits produced by the conversion electron.

We present an algorithm which, in a parameterized way, emulates the waveform digitization and pulse reconstruction in the calorimeter in the presence of pileup.

For the CE Monte Carlo, using the new algorithm increases the number of clusters in the CE peak [95 – 105] MeV by about 20-25%, compared to the present defaults.

12
13
14
15
16
17
18
19
20
21
22
23
24

Contents

1	Introduction	3
2	Mu2e calorimeter	3
3	Current model of digitization	3
4	Parametrization of the signal	4
4.1	Double pulse and pile-up	5
5	New algorithm	5
5.1	Implementation	5
5.2	Validation	6
5.2.1	Background generation	6
5.2.2	Algorithm validation	7
5.3	Results	8
6	Summary	10

25 1 Introduction

26 The Mu2e calorimeter readout is based on waveform digitization. Implementing the waveform
27 reconstruction requires developed infrastructure. To study effects of the pileup without such,
28 we implement an algorithm which, in a parametrized way, describes effects of both waveform
29 digitization and reconstruction. Parametrization provides convenient handles for the algorithm
30 tuning.

31 2 Mu2e calorimeter

32 The current design of the Mu2e calorimeter [6] provides a two-disk geometry, distant one from
33 each other 67 mm, both with an outer radius of 67 cm and an inner one of 36 cm [2].

34 Each disk is made up of ~ 1000 hexagonal prism shaped Lutetium Yttrium Orthosilicate
35 (LYSO) crystals with dimension 18.61 mm per side and 130 mm long [3], each one with two
36 readout APDs on the far side (Figure 1).

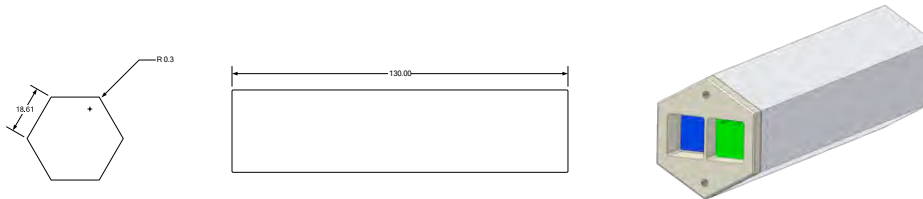


Figure 1: Dimensions for the hexagonal prism shaped LYSO crystals in the calorimeter and a 3D rendering of the crystal with the two APDs.

37 3 Current model of digitization

38 The current model of digitization is extremely simplistic: energy depositions closer than a con-
39 stant (set to 30 ns in the geometry file) are merged into one so-called calorimeter hit. It is
40 assumed that both APDs read out the same calorimeter hits.

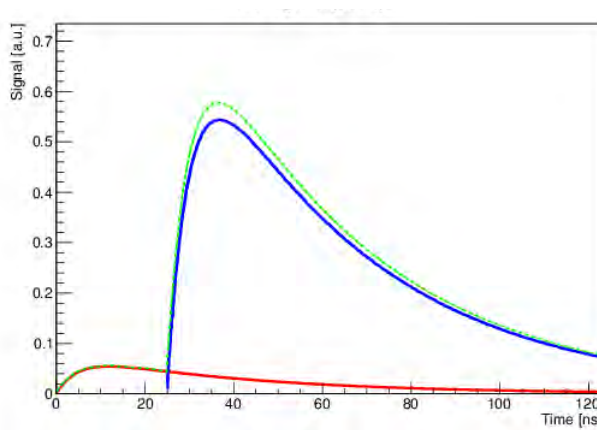


Figure 2: An example of two merged pulses with the current model of digitization: a background hit (in red) at $t = 0$ ns is merged with a conversion electron hit (in blue) at $t = 25$ ns. The total waveform is colored in green.

41 Next, crystal hits closer to each other than another constant (set to 100 ns in the source file)
 42 are merged into one so-called calorimeter crystal hit.

43 Energy of a crystal hit is determined by the time of its first calorimeter hit, the crystal hit
 44 energy is a sum of energies of the merged calorimeter hits.

45 Crystal hits are used as input for the calorimeter clustering algorithm.

46 So, there are two time constants with no direct physics meaning. They are also correlated,
 47 because the second one must be larger than the first one to be effective. In this way, tuning can
 48 become cumbersome and difficult to analyze.

49 Then, for example, a background hit at $t = 0$ ns could be merged with a conversion electron
 50 hit at $t = 100$ ns (Figure 2).

51 4 Parametrization of the signal

52 The signal coming from a scintillating inorganic crystal coupled with a photomultiplier has
 53 usually an exponential rising part, which depends on the electronics, and an exponential decay
 54 part, which depends on the properties of the crystal.

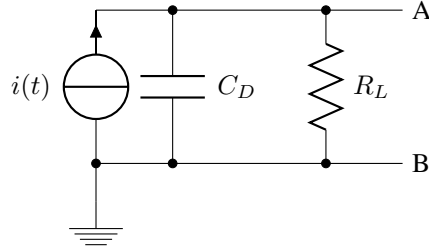


Figure 3: Circuitual scheme of a photomultiplier: an ideal current generator in parallel with a resistance and a capacitance.

55 In fact, a photomultiplier can be considered as an ideal current generator in parallel with a
 56 certain resistance and capacitance (Figure 3). So, the current at the anode will be given by [5]:

$$I(t) = A \cdot e^{-\frac{t}{\tau_D}} = \frac{V}{R_L} + C_D \frac{dV}{dT}.$$

57 This equation has the solution:

$$V(t) = A \cdot (e^{-\frac{t}{\tau_D}} - e^{-\frac{t}{\tau_R}}) = A \cdot e^{-\frac{t}{\tau_D}} (1 - e^{\frac{t}{\tau_D} - \frac{t}{\tau_R}}),$$

58 where $\tau_R = R_L C_D$ (Figure 4).

59 The LYSO crystal has a decay constant time $\tau_D \approx 40$ ns, while the flash ADCs used in the
 60 calorimeter readout have a rise constant time $\tau_R = R_L C_D = 50 \Omega \cdot 270 \text{ pF} = 13.5$ ns [8].

61 In our simulation these constants are set to $\tau_D = 40$ ns and $\tau_R = 10$ ns.

62 If APD is perfectly linear:

$$\int V(t) dt \propto E \Rightarrow A \propto \frac{E}{\tau_D - \tau_R}.$$

63 The time of the maximum of the function (leading-edge time) is given by:

$$64 t_1 = \frac{\tau_D \cdot \tau_R}{\tau_D - \tau_R} \cdot \ln\left(\frac{\tau_D}{\tau_R}\right) \approx 18.48 \text{ ns}.$$

65 In this parametrization, however, the timing resolution is not taken into account.

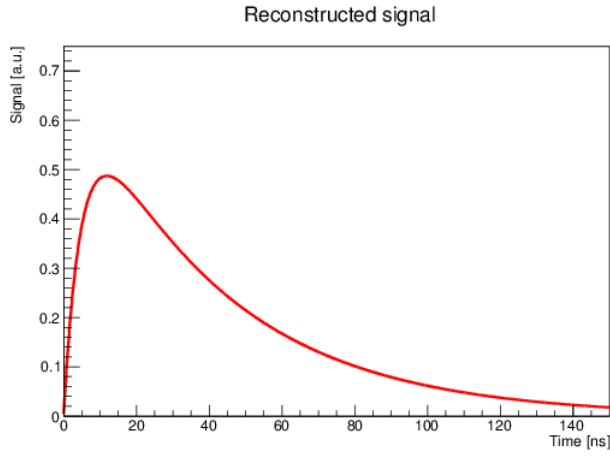


Figure 4: Waveform of a signal with $\tau_D = 40$ ns, $\tau_R = 10$ ns and $A = 1$.

66 4.1 Double pulse and pile-up

67 In case of two close in time pulses pile-up, the combined waveform function is given by:

$$V(t) = C_1 \cdot (e^{-\frac{t}{\tau_D}} - e^{-\frac{t}{\tau_R}}) + C_2 \cdot (e^{-\frac{t-\Delta t}{\tau_D}} - e^{-\frac{t-\Delta t}{\tau_R}}), \quad (1)$$

68 where Δt is the difference in time between the pulses.

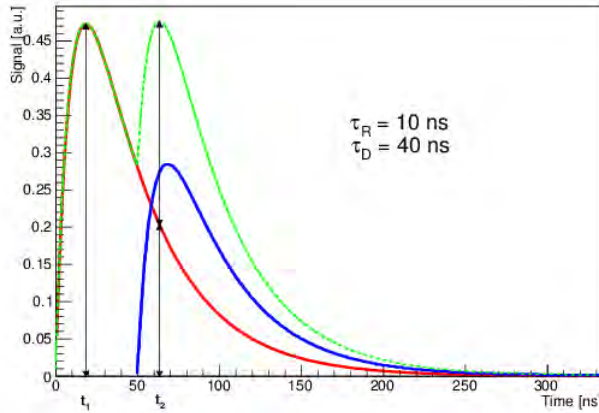


Figure 5: Simulation of the pile-up of two pulses. In green the sum of the waveforms.

69 For this function, the time of the second peak is given by (Figure 5):

$$t_2 = \ln\left(\frac{\tau_D}{\tau_R} \cdot \frac{1 + \frac{C_2}{C_1} \cdot e^{\frac{\Delta t}{\tau_R}}}{1 + \frac{C_2}{C_1} \cdot e^{\frac{\Delta t}{\tau_D}}}\right) \frac{\tau_D \cdot \tau_R}{\tau_D - \tau_R}.$$

70 5 New algorithm

71 5.1 Implementation

72 As an initial step, we effectively turn off merging of the Geant4 energy depositions by reducing
 73 the corresponding time constants from 30 ns down to 1 ns. For each crystal, there are 2 steps
 74 performed:

- 75 1. for a given crystal hit, represented by a function (1), merge with it all subsequent crystal
76 hits starting before the corresponding waveform reaches the maximum t_1 ;
- 77 2. two crystal hits separated in time by more than t_1 are considered separate if (see Figure
78 (6)) $A > k \cdot B$.

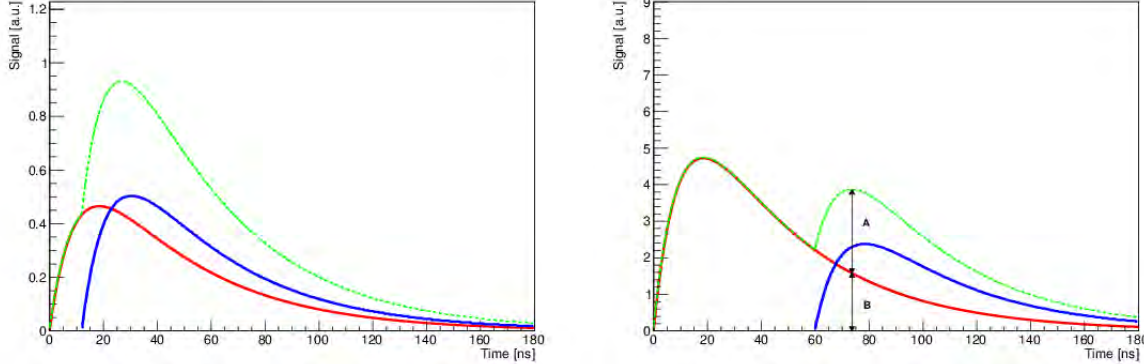


Figure 6: Examples of how the pile-up handling algorithm works: in the first graph the two pulses are merged because the second one arrives within the leading edge time t_1 , while in the second one the two pulses are resolved because $A > B$. A e B are calculated at $t = t_2$ and in this case $k = 1$.

79 So, the constants used now, τ_D and τ_R , have a direct physics meaning and their role is
80 well-defined. The merging constant k , moreover, can be used in order to take noise and photo-
81 statistics into account.

82 5.2 Validation

83 5.2.1 Background generation

84 In order to study the behavior of our algorithm and its differences from the previous model, we
85 generated a standard mix of background events needed for 1000 μ bunches [4] (Table 1). Offline
86 version 3.0.1 has been used.

87 In order to reduce the size of output files, only events which have at least one Geant4 step
88 point in the tracker or calorimeter are written out.

Background	Simulated events (millions)	Passed events per μ bunch
DIOs	20	161
Neutrons	38	542
Protons	3.2	36
Photons	63	355

Table 1: These are the numbers of simulated events needed for 1000 μ bunches [4] and the number of passed events per μ bunch.

89 These events are mixed with 1000 conversion electrons (one for each μ bunch) and then the
90 histograms for the energy and for the time distribution (Figure 7) are plotted.

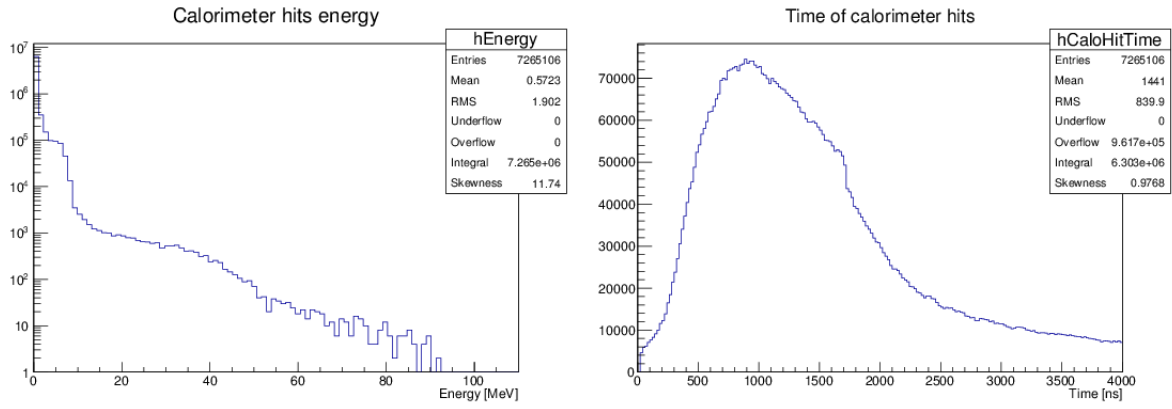


Figure 7: Time and energy distributions for 1000 μ bunches. The abrupt fall in the time distribution at $t \approx 1700$ ns is probably due to the missing wrap around of the tail in the next μ bunch.

91 5.2.2 Algorithm validation

92 In order to validate the algorithm, we plot a 2D histogram with the ratio of the amplitudes $\frac{B}{A}$ of
 93 the two signals on the horizontal axis and their time difference Δt on the vertical axis (Figure
 94 8). Three areas are clearly distinguishable:

- 95 • $t \gg 100$ ns and $\frac{B}{A} \gg 0.1$. The two signals are quite far in time and the second signal is
 96 not so smaller than the first one: they happen to be never merged. It corresponds to the
 97 green area of the plot in Figure 8.
- 98 • $t \ll 100$ ns and $\frac{B}{A} \ll 1$. The two signals are close time and the second signal is much
 99 smaller than the first one: they happen to be always merged. It corresponds to the red
 100 area of the plot in Figure 8.
- 101 • $t < t_1 \approx 18$ ns. The second signal arrives within the leading edge time t_1 , so it is always
 102 merged with the first one. It corresponds to the small empty area at the bottom of the plot
 103 in Figure 8.

$$A \cdot (e^{-\frac{t}{\tau_D}} - e^{-\frac{t}{\tau_R}}) + B \cdot (e^{-\frac{t-\Delta t}{\tau_D}} - e^{-\frac{t-\Delta t}{\tau_R}})$$

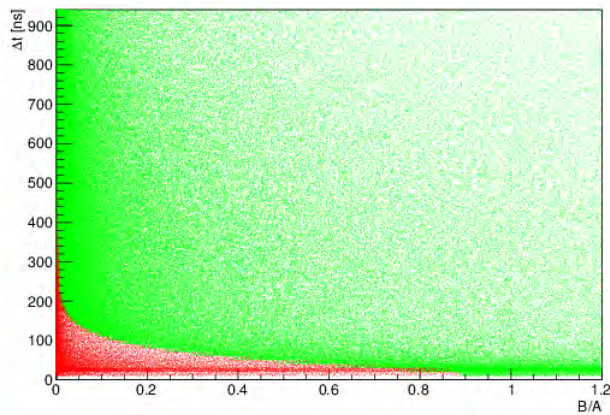


Figure 8: 2D histogram of the ratio of amplitudes $\frac{B}{A}$ against the time difference Δt for two signals.

104 Projections of the 2D histogram for every component (Figure 9 and 10) also provide useful
 105 information:

- 106 • for the merged pulses, the distribution of the ratio of amplitudes $\frac{B}{A}$ stops at ~ 0.9 : it
 107 means that when the second signal is bigger than ~ 0.9 times the first one, the algorithm
 108 never merges the pulses. In the time distribution, moreover, we can observe that there are
 109 merged pulses up to 600 ns distant in time from the first one;

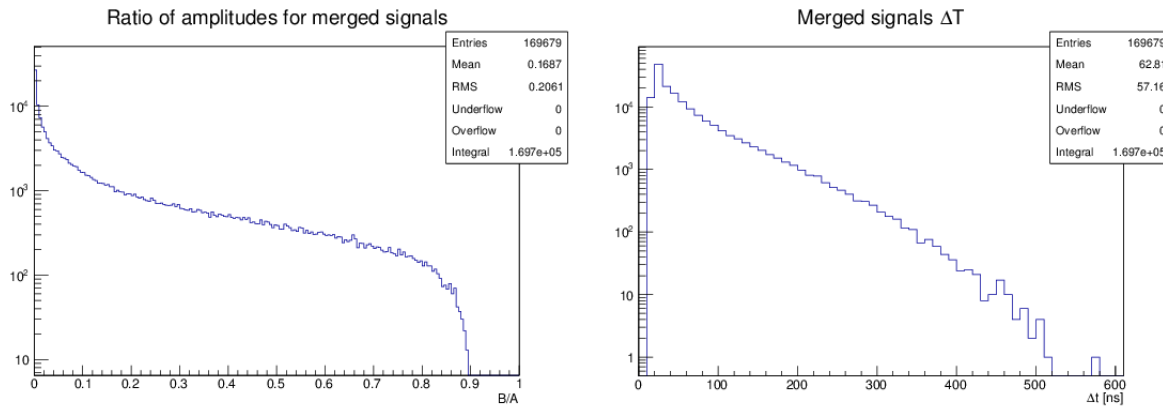


Figure 9: Projections of ratio of amplitudes $\frac{B}{A}$ and the time difference Δt for the merged signals.

- 110 • the projections for not merged pulses, instead, show that when the second pulse is bigger
 111 than the first one ($\frac{B}{A} > 1$) they are always resolved, as expected. In the time difference
 112 Δt distribution there is also a significant number of pulses separated by less than 100 ns,
 113 which shows that there are resolvable pulses very close in time,

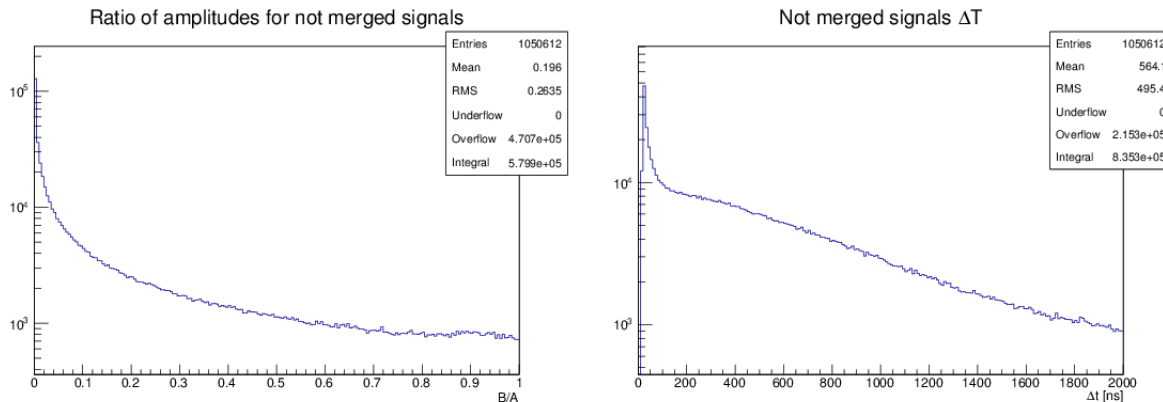


Figure 10: Projections of ratio of amplitudes $\frac{B}{A}$ and the time difference Δt for the resolved signals.

- 114 • the time distributions don't start at $t = 0$ in both cases because of the leading edge time
 115 merging (at $t_1 \approx 18$ ns).

116 5.3 Results

117 Our algorithm is validated looking to the result of clustering: in fact, pile-up affects the recon-
 118 struction in three ways:

- a background hit produced shortly before the conversion electron (CE) hit could get merged with it. As the timing of the merged pulse is determined by the first hit, the conversion electron hit would be lost for reconstruction;
- a background hit after the CE hit can be merged, adding the two corresponding energies;
- a background hit after the CE hit can be considered as a separate hit.

The old algorithm merges all the hits, if they are separated by less than 100 ns, otherwise it always merges them.

The new algorithm, for two pulses of the same height, reduces the merging time to $t_1 \approx 18$ ns and it could also merge a background hit after this time if it is sufficiently small. So, an increase is expected in the number of clusters around the energy of the CEs peak (~ 105 MeV), because there should be less CE hits merged with preceding background hits.

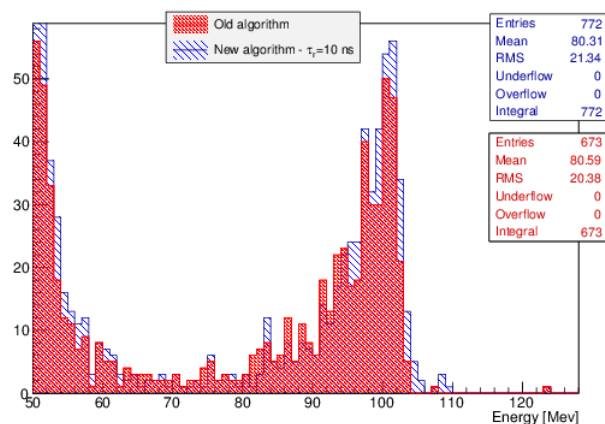


Figure 11: Histogram of the cluster energy distribution between 50 MeV and 120 MeV.

An effect of this improvement can be estimated as follows: for about 7000 hits in the calorimeter per μ bunch (the entries in Figure 7 divided by the number of μ bunches, 1000), there are $\sim 7/2 = 3.5$ hits per crystal per μ bunch (with the same occupancy for the two disks) and, for a μ bunch time of ~ 1700 ns, the hit frequency is ~ 2 MHz.

So, the probability to lose the most energetic crystal of the cluster is, with the current default settings of the hit reconstruction, $\frac{100}{500} = 20\%$, while with the new algorithm it should be $\frac{18}{500} = 3.6\%$.

The order of magnitude of the increase in the cluster energy around the CEs peak is then $O(10)\%$.

Plotting the cluster energy between 50 MeV and 120 MeV (Figure 11), we observe an increase in the interval $[50 - 60]$ MeV, which corresponds to the DIOs tail, a decrease in the $[60 - 80]$ MeV interval and an increase in the $[80 - 110]$ MeV interval: it means that the CE clusters moved to higher energies.

If the CEs peak is defined as the interval between 95 MeV and 105 MeV, the increase in the number of events in the peak is 24%. Instead, if the rising time constant τ_R is reduced by a factor of 2 (from 10 ns to 5 ns), corresponding a leading edge time $t_1 \approx 11.88$ ns, the increase is 25%: the additional improvement is quite small.

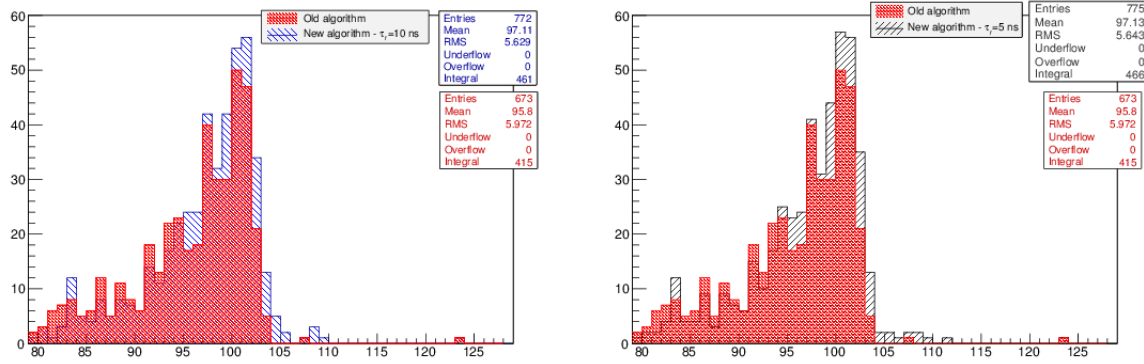


Figure 12: Cluster energy histograms for $\tau_R = 10$ ns (on the left) and for $\tau_R = 5$ ns (on the right). The increase of the number of clusters in the interval $[95 - 105]$ MeV is, respectively, 24 % and 25 %.

6 Summary

We implemented a new algorithm, which in a parameterized way describes the digitization and reconstruction. The obtained increase in the number of clusters in the energy interval $[95 - 105]$ MeV, which corresponds to the conversion electron peak, is 24 %. The algorithm is implemented in the `MakeCaloCrystalHitsNew` module, available in the CVS repository. The constants used, τ_D and τ_R , have now a direct physics meaning and can be directly modified in the `fcl` configuration file of the job.

Further reduction of the pulse leading edge $t_1 = \frac{\tau_D \cdot \tau_R}{\tau_D - \tau_R} \cdot \ln\left(\frac{\tau_D}{\tau_R}\right)$, which depends of the flash ADCs used, results in only a marginal improvement.

156 **References**

- 157 [1] Mu2e collaboration. *Mu2e Conceptual Design Report*. Mu2e DocDB, 1169.
- 158 [2] S. Groetsch, A. Laha, and P. Murat. *Optimization of the Disk-Based Calorimeter Geometry:*
159 *Choice of the Inner Radius*. Mu2e DocDB, 3189.
- 160 [3] D. G. Hitlin. *Prototype LYSO Crystal Specifications*. Mu2e DocDB, 2984.
- 161 [4] R. Kutschke. *Event Mixing Update*. Mu2e DocDB, 2351.
- 162 [5] W.R. Leo. *Techniques for Nuclear and Particle Physics Experiments: A How-To Approach*.
163 Springer, 1994.
- 164 [6] S. Miscetti. *Calorimeter Status and plan*. Mu2e DocDB, 2893.
- 165 [7] G. Onorato. *Upgrade on calorimeter background simulations*. Mu2e DocDB, 2297.
- 166 [8] I. Sarra. *Pile up rejection capability with respect to ADCs time resolution*. Mu2e DocDB,
167 2299.